



FULL PAPER

Quantum chemical study of the Jahn – Teller effect on the distortions of XO_2 ($X = O, S, Se, Te$) systems

Ali Esmaili^a  | Reza Fazaeli^{b,*}  | Esmat Mohammadi Nasab^a^aDepartment of Chemistry, Arak Branch, Islamic Azad University, Arak, Iran^bDepartment of Chemistry, South Tehran Branch, Islamic Azad University, P.O. BOX 11365-4435, Tehran, Iran

Preliminary researches provided essential information about the optimized configuration of triatomic XO_2 ($X = O, S, Se, Te$) systems, which were bent in the ground state and linear in their first excited state. The Jahn-Teller effects including the Jahn-Teller (JTE), the Renner-Teller effect (RTE), and the pseudo Jahn-Teller effect (PJTE) are parts of the most important reasons for structural distortion in the high symmetry configurations for each molecular system. This study purpose was to investigate the dependence between PJT parameters including the vibronic coupling constant values (F), energy gap between reference states (Δ), and initial force constant (K_0). In all above mentioned molecules, stability were increased with the reduction in the symmetry level. This increment was attributed to the PJTE. The vibronic coupling interaction between the ground (Σ_g), and the first excited states (Π_u) through the PJTE problem ($PJT(\Sigma_g + \Pi_u) \times \Pi_u$) was because of the asymmetry and molecules bending phenomenon. The hardness difference parameter $\Delta[\eta(C_{2v}) - \eta(D_{\infty h})]$ decreases from O to Te (30.42, 22.66, 22.65, 22.58 Kcal/mol). These changes could explain the trend, which were observed for the $D_{\infty h} \rightarrow C_{2v}$ conversion process.

***Corresponding Author:**

Reza Fazaeli

Email: r_fazaeli@azad.ac.ir

Tel.: +98 (21) 77248534

KEYWORDS

The Jahn-Teller effect; vibronic interactions; Ab initio; quantum; symmetry breaking.

Introduction

Despite of the triatomic systems' apparent simplicity, the origin of their equilibrium geometry is not still entirely known. Preliminary researches provided essential information on these specific molecular systems' optimized configuration, but this information cannot explain the geometric origin and the difference in configurations directly; specifically, the electron structure calculations by its own cannot explain why many of the triatomic systems (such as SiH_2^+ , H_2O^+ , CH_2^+ , HNO^+ , HNF , HBF , ...) are bent in the ground state, and also are linear in the first excited state [1]. So many models have been used in many studies like Walsh diagrams and molecular orbital theory, the

valence shell electron pair repulsion model (VSEPR), polarized ion models as well as the softness hardness-based models, but they cannot totally explain about this issue, [2].

The triatomic molecules and free radicals extensive application has been of interest in combustion, photochemical, atmospheric chemistry, interstellar chemistry processes, and frequently considered as intermediate in chemical reactions [3-7].

The vibronic coupling theory gives us information about the molecules shape. It is popular that the Jahn-Teller effect (JTE) (including the Jahn-Teller, which is suitable for the systems in the electronically degenerate states, the Renner-Teller effect (RTE) which is designed for the linear molecules, and the pseudo Jahn-Teller effect

(PJTE), which is applied to each system in degenerate and nondegenerate states) is the only structural distortion source from the high symmetry configurations for each molecular system [8-9]. Consequently, it seems normal to attribute the bending distortion of the triatomic and the linear molecular systems in the electronically degenerate states for effecting (RTE). Nevertheless, despite of the JTE, RTE, and PJTE efficacy as the only high symmetry configurations instability sources for each multi-atom system, there is no rigorous proof introducing the RTE as the only linear configurations instability source.

Asymmetry would occur in the high symmetry configuration because of the ground and excited electron states mixing in a molecule [8-15]. In a two-level problem, the ground and excited electron states of good behavior are due to an orthogonal nuclear configuration; therefore, the ground and excited electron states integration does not take place. The ground and excited electron states are mixed and can no longer be orthogonal according to the nuclear displacement (Q). This mixing depends on the electron wave functions from the ground (Ψ_1) and excited states (Ψ_2).

The initial force constant (constant force without K_0 , PJTE) is defined from the ground state in the Q direction for each of the multi-atom system in a high symmetry configuration.

$$K_0 = \langle \Psi_1 | \left(\frac{\partial^2 H}{\partial Q^2} \right)_0 | \Psi_2 \rangle \quad (1)$$

Where H is Hamiltony. It is noteworthy to say that, for each multi-electron system, the PJTE free force constant is positive [8-9] and it can be shown that nuclear displacement (Q) leads to the mixing of the ground and the excited states, and the force constant decreases in the configuration with the highest symmetry.

$$K = K_0 - \left(\frac{F^2}{\Delta} \right) \quad (2)$$

Where F is the vibronic coupling constant and Δ is the energy gap between the two reference states.

$$F = \langle \Psi_1 | \left(\frac{\partial H}{\partial Q} \right)_0 | \Psi_2 \rangle \quad (3)$$

If it is $\frac{F^2}{\Delta} > K$, $K < 0$, and the system is unstable in the Q direction, and many of the excited states help K, their effects are summarized, and a multi-level problem is going to be created [6,8-9].

Garcia Fernandez *et al.* (2007) studied on the linear and nonlinear nature of ML_2 molecules and outlined the PJTE results. Various models like covalence, metal core polarization, hybridization, and VSEPR were used in this research, and the PJTE referred to as the instability sole source of the high symmetry system in non-degenerate conditions [16]. Yang Liu and Bersuker indicated that RTE cannot be the only source, since PJTE is more effective on these molecules curvature for linear molecules with electronically degenerate states [12]. PJTE for the curvature is more important than some of the triatomic molecules, which were expressed by Hakan, Bersuker, and Boggs (2012). They showed that the PJTE is the only triatomic molecule instability source in a linear state. These results may state that PJTE plays a special role in all linear molecular systems instability [17]. Yang Liu (2014) carried out a research on some triatomic molecules curvature. They found that PJTE causes the curvature in the linear highest symmetric configuration of the triatomic systems between the ground and the excited states [18]. Many computational investigations on the structure and properties of molecules in their electronically excited states have been reported [19-30].

The purpose of this study was to investigate PJTE in the vibronic coupling between the ground state and several excited states of XO_2 ($X = O, S, Se, Te$) compounds. Ab initio explains the instability, the distortions of linear highest-symmetric configuration, and the curved configuration production origin.

Any structural distortion of a polyatomic system is a consequence of the JT, PJT or RT effects. Several theoretical investigations have been published about pseudo Jahn–Teller (PJT) distortions in organic and inorganic compounds [31-35].

Computational methods

This study investigated the dependence between the PJTE parameters (the vibronic coupling constant values (F), energy gap between reference states (Δ), and initial force constant (K_0)). The configuration properties, global hardness, global electronegativity, and natural loads of XO_2 compounds ($X = O, S, Se, Te$) were attained by means of time-dependent density functional theory (TD-DFT) (LC-wPBE / Def2-TZVPP, B3LYP / Def2-TZVPP) [15, 36-37].

Gaussian program 09 [38], and the theoretical levels of B3LYP / Def2-TZVPP and LC-wPBE / Def2-TZVPP were used in order to optimize the ozone structure (**1**), sulfur dioxide (**2**), selenium dioxide (**3**), and tellurium dioxide (**4**) in the linear ($D_{\infty h}$ symmetry) and in curved states (C_{2v} symmetry) [39]. The compounds stability in the linear configuration is calculated and compared, the optimizing and calculating the frequency of XO_2 compounds in negative frequency linear configurations ($D_{\infty h}$ symmetry) along with the distortion coordinate (Πu). The ground and excited states of the compounds' normal stabilization points were determined using the negative frequencies, and also the compounds electron structures were studied in the linear ($D_{\infty h}$ symmetry), and curved states (C_{2v} symmetry) by TD-DFT. Stabilization energy, non-diagonal elements, bonding and antibonding the orbital

energy, electron delocalization $LP \rightarrow \sigma^*$, natural bond orders(NBO) , and normal atomic charges in the XO_2 compounds curved structure were analyzed by using the NBO.6 program [40].

There is a significant relationship between the donor-acceptor stabilization energy with the electron delocalization and the orbital S overlap, and also an inverse insignificant relationship between the electron delocalization's stabilization energy and the energy difference between the donor orbital (i) and the acceptor orbital (j) ($\frac{1}{\Delta E}, \Delta E = \varepsilon_j - \varepsilon_i$) [41]. Consequently, the donor(i)-acceptor (j) stabilization energy(E_2) are estimated according to the Equation (4).

$$E_2 = q_i \frac{F^2(i,j)}{\varepsilon_j - \varepsilon_i} \quad (4)$$

Where q_i is the donor occupied orbital, ε_i and ε_j are the diagonal elements (orbital energy), $F_{i,j}$ is the nondiagonal element, $F_{i,j}$ is the nondiagonal element, which is dependent on the orbital S overlapping integral directly. The large values of E_2 indicate an interaction between the donor and acceptor electrons.

Results and discussion

Energy aspects

Tables 1 and 2 displayed differences in electron energy ($E_0 = E_{ele} + ZPE$) between $D_{\infty h}$ and C_{2v} configurations from the compounds **1** to **4**, optimized with the B3LYP / Def2-TZVPP and LC-wPBE / Def2-TZVPP theory levels. Also, the zero point energy (ZPE) and energy parameters $\Delta [ZPE (D_{\infty h}) - ZPE (C_{2v})]$ of $D_{\infty h}$ and C_{2v} configurations for compounds **1** to **4** are summarized in the Tables 1 and 2 as followings:

TABLE 1 G, H, E₀ (hartree) and S (cal mol⁻¹k⁻¹) in 298k and 1 atm, ΔH, ΔG, ΔE₀ parameters (kcal mol⁻¹) and ΔS (cal mol⁻¹K⁻¹) for the (C_{2v}) and linear (D_{∞h}) structures and also for the bond dissociation processes of compounds 1 to 4

LC-wPBE/Def2-TZVPP										
	ZPE	E ₀	H	S	G	ΔZPE	ΔE ₀	ΔH	ΔS	ΔG
Geometries										
1, C _{2v} ; (\bar{X}^1A_1)	0.008125	-225.364627	-225.360756	56.652	-225.387673	0.00	0.00	0.00	0.000	0.00
1, D _{∞h} ; ($\bar{X}^1\Sigma_g^+$)	0.005980	-225.228830	-225.225042	52.549	-225.250010	-1.35	85.21	85.16	-4.103	86.38
O ₃ →O ₂ +O; ($^3A''$)	0.004226	-225.332634	-225.327170	72.904	-225.361809	-2.45	20.08	21.08	16.252	16.23
2, C _{2v} ; (\bar{X}^1A_1)	0.007477	-548.491159	-548.487170	59.172	-548.515285	0.00	0.00	0.00	0.000	0.00
2, D _{∞h} ; ($\bar{X}^1\Sigma_g^+$)	0.005676	-548.382175	-548.378834	52.395	-548.403728	-1.13	68.39	67.98	-6.777	70.00
SO ₂ →SO+O; ($^3A''$)	0.002932	-548.283726	-548.279054	71.692	-548.313117	-2.85	130.17	130.59	12.52	126.86
3, C _{2v} ; (\bar{X}^1A_1)	0.005868	-2551.566179	-2551.562039	62.477	-2551.591723	0.00	0.00	0.00	0.000	0.00
3, D _{∞h} ; ($\bar{X}^1\Sigma_g^+$)	0.004285	-2551.448650	-2551.445252	54.716	-2551.471250	-0.99	73.75	73.29	-7.761	75.60
SeO ₂ →SeO+O; ($^3A''$)	0.002381	-2551.270734	-2551.266019	72.868	-2551.300641	-2.19	185.39	185.76	10.391	182.6
4, C _{2v} ; (\bar{X}^1A_1)	0.005107	-418.389865	-418.385596	64.869	-418.416418	0.00	0.00	0.00	0.000	0.00
4, D _{∞h} ; ($\bar{X}^1\Sigma_g^+$)	0.003882	-418.283161	-418.279727	56.344	-418.306498	-0.77	66.96	66.43	-8.525	68.98
TeO ₂ →TeO+O; ($^3A''$)	0.002242	-418.249024	-418.244395	74.234	-418.279666	-1.80	88.38	88.61	9.365	85.81

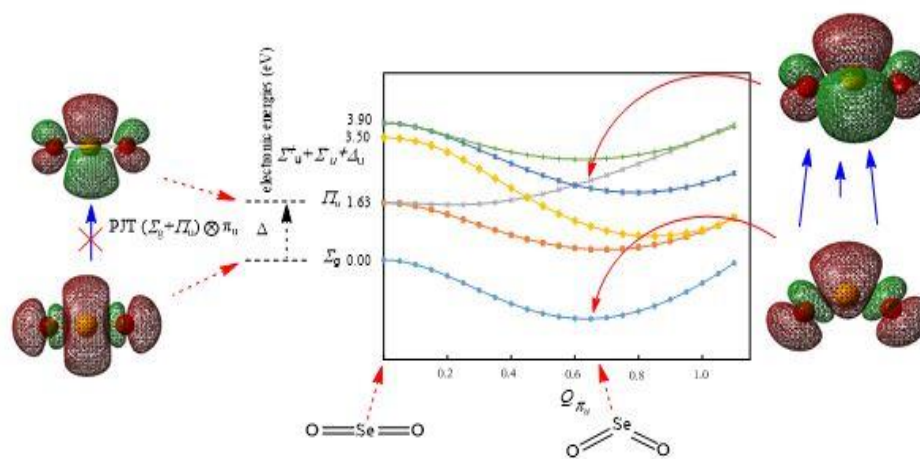
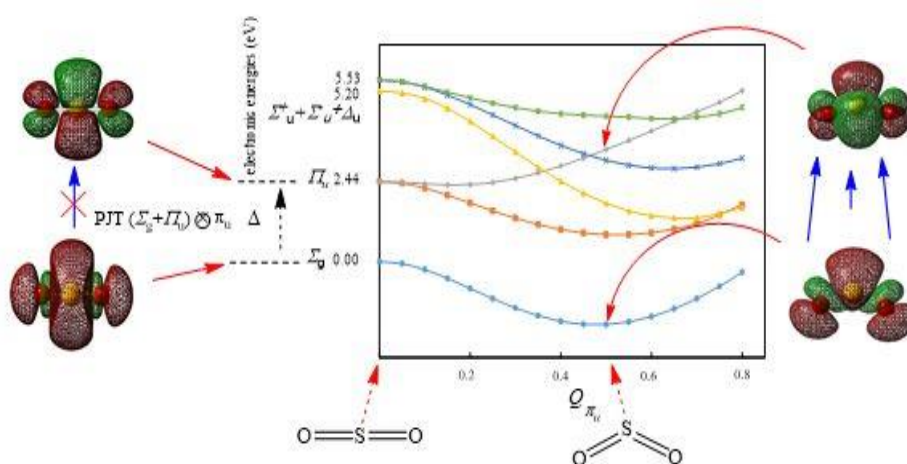
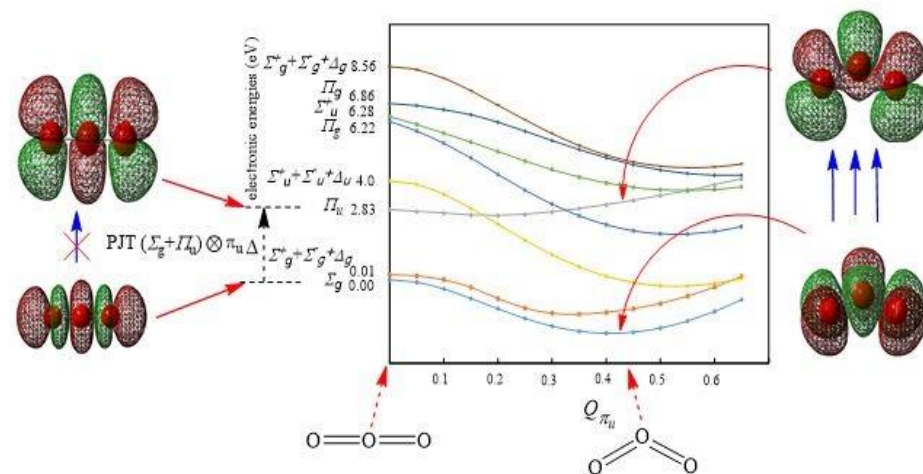
TABLE 2 G, H, E₀ (hartree) and S (cal mol⁻¹k⁻¹) in 298k and 1 atm, ΔH, ΔG, ΔE₀ parameters (kcal mol⁻¹) and ΔS (cal mol⁻¹K⁻¹) for the (C_{2v}) and linear (D_{∞h}) structures and also for the bond dissociation processes of compounds 1 to 4

B3LYP/Def2-TZVPP										
	ZPE	E ₀	H	S	G	ΔZPE	ΔE ₀	ΔH	ΔS	ΔG
Geometries										
1, C _{2v} ; (\bar{X}^1A_1)	0.007308	-225.504945	-225.501044	56.839	-225.528050	0.00	0.00	0.00	0.000	0.00
1, D _{∞h} ; ($\bar{X}^1\Sigma_g^+$)	0.005330	-225.376685	-225.372813	52.992	-225.397991	-1.24	80.48	80.47	-3.847	81.61
O ₃ →O ₂ +O; ($^3A''$)	0.003853	-225.466836	-225.462245	67.299	-225.494221	-2.17	23.91	24.35	10.46	21.23
2, C _{2v} ; (\bar{X}^1A_1)	0.007002	-548.715427	-548.711415	59.305	-548.739593	0.00	0.00	0.00	0.000	0.00
2, D _{∞h} ; ($\bar{X}^1\Sigma_g^+$)	0.005113	-548.616472	-548.613110	52.511	-548.638059	-1.19	62.10	61.69	-6.794	63.71
SO ₂ →SO+O; ($^3A''$)	0.002718	-548.512921	-548.508256	71.363	-548.542162	-2.69	127.07	127.48	12.058	123.89
3, C _{2v} ; (\bar{X}^1A_1)	0.005352	-2552.030569	-2552.026377	62.741	-2552.056187	0.00	0.00	0.00	0.000	0.00
3, D _{∞h} ; ($\bar{X}^1\Sigma_g^+$)	0.003762	-2551.932176	-2551.928729	54.946	-2551.954835	-1.00	61.74	61.28	-7.795	63.60
SeO ₂ →SeO+O; ($^3A''$)	0.002254	-2551.757272	-2551.752572	71.965	-2551.786764	-1.94	171.50	171.82	9.224	169.07
4, C _{2v} ; (\bar{X}^1A_1)	0.004672	-418.550286	-418.545960	65.180	-418.576929	0.00	0.00	0.00	0.000	0.00
4, D _{∞h} ; ($\bar{X}^1\Sigma_g^+$)	0.003344	-418.463511	-418.460006	56.639	-418.486917	-0.83	54.45	53.94	-8.541	56.48

The vibronic analysis is displayed in the D_{∞h} symmetry with 4 negative frequencies. These frequencies and their force constant values were summarized in Table 3. The vibronic modes symmetry of the negative frequencies are presented in Figure 1. The vibronic modes would change the molecular symmetry from the linear (D_{∞h}) to the curved state (C_{2v}). The configurations distortion with the highest symmetry (D_{∞h}) of compounds from **1** to **4** are because of the PJTE [42-44]. These distortions' main shares from configurations with the highest symmetry (D_{∞h}) to (C_{2v}) the corresponding compounds symmetry are mainly because of the PJTE mixing the ground (Σ_g) with the excited states (Π_u). The mixing of Ψ_{HOMO} (Σ_g) and Ψ_{LUMO} (Π_u)

orbitals in these compounds is because of the PJTE two-level problem ($\Sigma_g + \Pi_u$) × Π_u .

The ground and excited states energy, and their variations during the distortion coordinate (Q_{Π_u}) is displayed in Figure 1. The lower curve curvature (belonging to the electron configuration in the ground state) is negative from the adiabatic potential energy surface (APES), but the second curve has a positive curvature from compounds **1-4** (belonging to the excited state of the electron configuration that interacts with the ground state curve with respect to the displacement Q_{Π_u}). Investigating the above mentioned excited electron states shows that they cannot contribute in the PJTE interaction in compounds **1-4** (Figure 1).



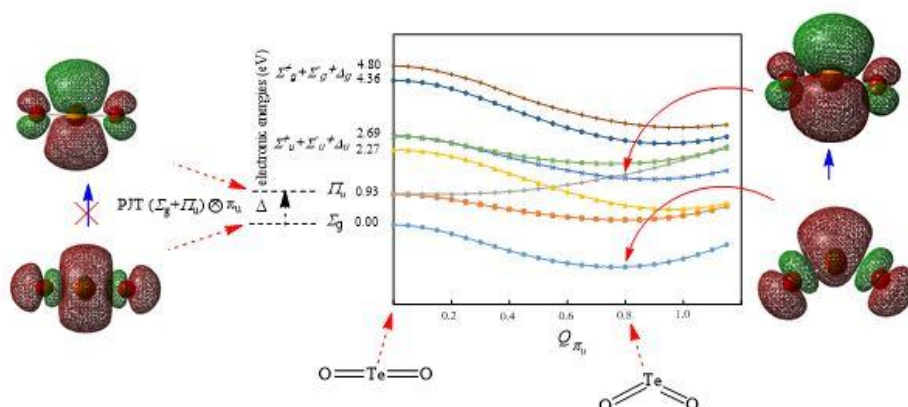


FIGURE 1 TD-DFT (LC-wPBE / Def2-TZVPP) energy curves (in eV) of the ground and excited states in the bending directions of compounds 1-4. For the liner structures, the symmetries of the electron-induced states involved in the vibronic coupling

The energy gap between the desired states (Δ) decreases during the distortion coordinate from compounds **1-4** (2.83, 2.34, 1.40, and 0.62, respectively). By the reduction of Δ values in the linear configuration ($D_{\infty h}$) of these compounds, the PJTE stabilization

energy also decreases for the distortion of $D_{\infty h} \rightarrow C_{2v}$. After that, the F_{ij} vibronic coupling constant is also reduced by the reduction of the energy gap between the ground and excited states (Δ) from compounds **1-4** (Table 3).

TABLE 3 Calculating vibrational frequencies (cm^{-1}) of compounds 1-4

Compound	O ₃	SO ₂	SeO ₂	TeO ₂
Force Const.	12.694	8.788	4.981	3.535
Δ	2.83	2.34	1.40	0.62
ν_1	-1160.64	-836.35	-638.51	-556.88
F_{ij}	0.222	0.194	0.181	0.148

LC-wPBE/Def2-TZVPP B3LYP/Def2-TZVPP

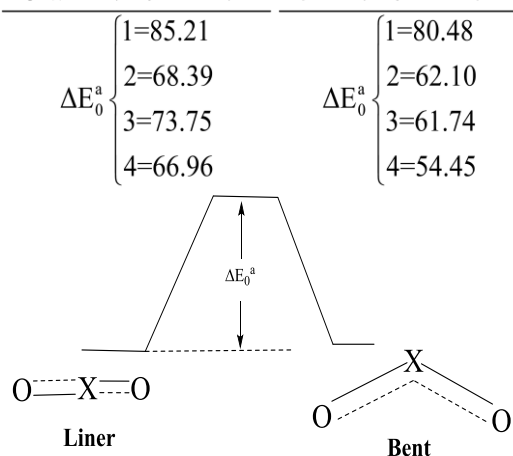


FIGURE 2 Calculated energy profiles of the linear configuration interconversions of compounds 1-4 via their corresponding curved forms (ΔE_0^a in Hartree)

Structural parameters

The O-X bonding spacing and the O-X-O bonding angle are listed in Table 4. The bonding spacing in the C_{2v} symmetry is shorter in comparison with the $D_{\infty h}$ symmetry. Also, the O-X-O bonding angle decreases by the reduction of the symmetry (Table 4). All the methods' results were used in order to show that the difference in bonding length was calculated between the O-X bonding in the bent and the linear configurations $\Delta [r_{O-X(D_{\infty h})} - r_{O-X(C_{2v})}]$ decreases from the compounds **1** to **2** and, after that, from compounds **2** to **4** have increase (0.033, 0.011, 0.045, 0.053 for compounds **1-4**, respectively).

TABLE 4 B3LYP / Def2-TZVPP (a), B3LYP / TZP (b), LC- ω PBE / Def2-TZVPP (c) and LC- ω PBE / TZP (d) calculated structural parameters of the bent (C_{2v}) ground state and linear ($D_{\infty h}$) structures of compounds 1-4.

State	1		2		3		4	
	C_{2v}	$D_{\infty h}$	C_{2v}	$D_{\infty h}$	C_{2v}	$D_{\infty h}$	C_{2v}	$D_{\infty h}$
Bond lengths (\AA)								
r_{M-M}	(1.254) ^a	(1.294) ^a	(1.439) ^a	(1.457) ^a	(1.612) ^a	(1.669) ^a	(1.795) ^a	
	(1.254) ^b	(1.293) ^b	(1.452) ^b	(1.484) ^b	(1.609) ^b	(1.664) ^b	(1.811) ^b	
	(1.230) ^c	(1.263) ^c	(1.423) ^c	(1.434) ^c	(1.585) ^c	(1.630) ^c	(1.762) ^c	
	(1.230) ^d	(1.262) ^d	(1.436) ^d	(1.457) ^d	(1.578) ^d	(1.619) ^d	(1.774) ^d	
	(1.278 \pm 0.002) ^g		(1.4343 \pm 0.0003) ^e					
	(1.278) ^h		(1.431 \pm 0.002) ^f					
	(1.27276) ⁱ							
$\Delta[r_{M-M}(D_{\infty h})-r_{M-M}(C_{2v})]$ ^d	0.032		0.021		0.041		0.073	
Bond angles ($^{\circ}$)								
	(118.3) ^a	(180.0) ^a	(119.0) ^a	(180.0) ^a	(113.8) ^a	(180.0) ^a	(110.2) ^a	(180.0) ^a
	(118.2) ^b	(180.0) ^b	(117.7) ^b	(180.0) ^b	(114.1) ^b	(180.0) ^b	(107.8) ^b	(180.0) ^b
	(117.8) ^c	(180.0) ^c	(118.9) ^c	(180.0) ^c	(113.7) ^c	(180.0) ^c	(110.2) ^c	(180.0) ^c
θ_{b-x-o}	(117.7) ^d	(180.0) ^d	(117.7) ^d	(180.0) ^d	(113.8) ^d	(180.0) ^d	(107.3) ^d	(180.0) ^d
	(116.45 \pm 0.30) ^g		(119.5 \pm 0.3) ^e					
	(116.82) ^h							
	(116.75) ⁱ							

^eFrom electron diffraction, C.H. Holder, Jr. and M. Fink, J. Chem. Phys., 75 (11), 5323-5325 (1981). ^fFrom Electron-diffraction, A. H. Clark, B. Beagley, Transactions of the Faraday Society, 67, 2216-2224 (1971). ^gFrom microwave spectroscopy, R. H. Hoghes, J. Chem. Phys. 24 (1), 131-138 (1956). ^hFrom microwave spectroscopy, R. Trambarulo, S. N. Ghosh, C. A. Burrus, Jr. and W. Gordy, J. Chem. Phys., 21, 851 (1953). ⁱFrom high resolution infrared spectroscopy, VG Tyuterev, S. Tashkun, P.Jensen, A. Barbe and T. Cours, J. Mol. Spectrosc., 198, 57- (1999)

Global hardness and electronegativity

The highest occupied molecular orbital (HOMO) and the lowest unoccupied molecular orbital (LUMO) energies are calculated by the C_{2v} and $D_{\infty h}$ configurations in compounds **1** to **4** with the LC- ω PBE/Def2-TZVPP theory surface (Table 5). The values of ϵ_{HOMO} increase in the C_{2v} configuration from compounds **1** to **4**, but the values of ϵ_{LUMO} show reduction in the C_{2v} configuration from compounds **1** to **2**, followed by increases from compounds **2** to **4**. Moreover, the energy gap between HOMO and LUMO orbitals ($\epsilon_{LUMO} - \epsilon_{HOMO}$) in the C_{2v} and $D_{\infty h}$ configurations increases from compounds **1** to **2**, followed by decreases from compound **2** to **4**. The harder configuration is more stable in a molecule, and consequently the soft configuration is less stable, which is consistent with the maximum hardness principles. Here, we describe the molecular hardness by two relationships. According to the Koopman's theorem, hardness is defined as the energy gap between the HOMO and LUMO.

$$\eta = 0.5 (\epsilon_{LUMO} - \epsilon_{HOMO}) \quad (5)$$

Also, the following relationship is established between the molecule global hardness (η), as well as its corresponding ionization potential (I) and electron affinity (A).

$$\eta = 0.5 (I - A) \quad (6)$$

According to the information of Table 5, the global hardness values of the curved geometric (C_{2v}), and linear ($D_{\infty h}$) configurations increases in compounds **1** to **2**, and after that decreases from compounds **2** to **4**. This results indicated that the bent configuration of (C_{2v}) in compounds **1** to **4** is harder than the linear configuration ($D_{\infty h}$). Accordingly, the curved form (C_{2v}) is more stable than the linear form ($D_{\infty h}$) from compounds **1** to **4** [45-48].

We calculate the parameter $\Delta[\eta(C_{2v}) - \eta(D_{\infty h})]$ using the attained hardness values. The parameter $\Delta[\eta(C_{2v}) - \eta(D_{\infty h})]$ decreases from the compounds **1** to **4**. These changes can explain the trend observed for the $D_{\infty h} \rightarrow C_{2v}$ conversion process. Therefore, ZEP values decrease from compounds **1** to **4** in the

curved (C_{2v}) and linear ($D_{\infty h}$) configurations. However, the variations in the ZEP difference show an increasing trend between the Δ [ZEP (C_{2v}) - ZEP ($D_{\infty h}$)] structures from compounds **1** to **4**. The results of this research presented that the global electronegativity values in the curved configuration (C_{2v}) are greater than the linear configuration ($D_{\infty h}$) during compounds of **1** to **4** (Table 5). According to these values, it can be said that the Lewis acid and Lewis base characteristic determine the global electronegativity. A molecule with a larger value is identified as a strong Lewis acid and a molecule with a

smaller value is known as a strong Lewis base. As a result, compound **1** is considered as a stronger Lewis acid, and compound **4** as a stronger Lewis base amongst the compounds of **1** to **4**. The Δ parameter is determined as $\Delta[\chi(C_{2v}) - \chi(D_{\infty h})]$ using the global electronegative values for the C_{2v} and $D_{\infty h}$ configurations. It is remarkable that when the parameter $\Delta[\chi(C_{2v}) - \chi(D_{\infty h})]$ is calculated, we found that this parameter decreases from compounds **1** to **4**, and this reduction process corresponds with the decrease in the PJTE stabilization energy during the $D_{\infty h} \rightarrow C_{2v}$ conversion process

TABLE 5 LC- ω PBE / TZP calculated energy (in au) of HOMO, LUMO, LUMO-HOMO (in au), global hardness (η , in au), global softness (S , in au), $\Delta\eta$ (in kcal mol⁻¹) and ΔS (in au) parameters for the bent (C_{2v}) ground state and linear ($D_{\infty h}$) structures of compounds 1-4

Geometry	ϵ_{HOMO}	ϵ_{LUMO}	$\epsilon_{\text{LUMO}} - \epsilon_{\text{HOMO}}$	I	A	η	χ	$\Delta\eta$	$\Delta\chi$
1 , C_{2v}	-0.46008	-0.08132	0.37876	0.46008	0.08132	0.18938	0.27070	0.04847(30.42) ^a	0.04717(29.60) ^a
1 , $D_{\infty h}$	-0.36443	-0.08262	0.28181	0.36443	0.08262	0.14091	0.22353	0.00000	0.00000
2 , C_{2v}	-0.45115	-0.03602	0.41513	0.45115	0.03602	0.20757	0.24359	0.03611(22.66) ^a	0.04167(26.15) ^a
2 , $D_{\infty h}$	-0.37338	-0.03046	0.34292	0.37338	0.03046	0.17146	0.20192	0.00000	0.00000
3 , C_{2v}	-0.43622	-0.06565	0.37057	0.43622	0.06565	0.18529	0.25094	0.03609(22.65) ^a	0.02603(16.33) ^a
3 , $D_{\infty h}$	-0.37411	-0.07571	0.29840	0.37411	0.07571	0.14920	0.22491	0.00000	0.00000
4 , C_{2v}	-0.41909	-0.08823	0.33086	0.41909	0.08823	0.16543	0.25366	0.03599(22.58) ^a	0.02164(13.58) ^a
4 , $D_{\infty h}$	-0.36146	-0.10258	0.25888	0.36146	0.10258	0.12944	0.23202	0.00000	0.00000

Stabilization energies associated with the electron delocalizations

Despite the fact that studying the stabilization energies associated with the electron delocalizations $LP(3)_{O_3} \rightarrow \sigma_{X_2-O_3}^*$, a NBO analysis was used in the $D_{\infty h}$ components **1** to **4** configuration, Figure 1 indicated that the PJTE stabilization energy decreases from compound **1** to **4**. The molecular orbital analysis displays that PJTE is associated to the ground electron (Σ_g) and excited states (Π_u) mixing and also connected to the mixing of HOMO (+1) (Π_u) and LUMO (Σ_g). It should be noted that the PJT distortion in the compounds **1-4** linear configuration ($D_{\infty h} \rightarrow C_{2v}$) along with the Π_u displacement is because of the reduction in the symmetry mixing the orbital Σ_g and Π_u with Π_u . The results of the NBO analysis indicate a

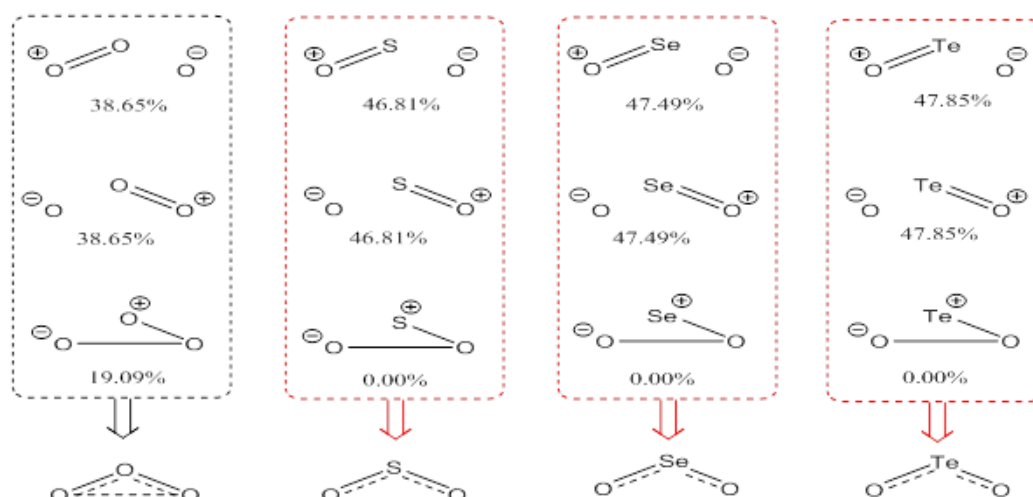
reduction in the electron delocalizations of the curved structure (C_{2v}) from compounds **1** to **2**, and after that increasing from compounds **2** to **4** (Table 6).

Natural charges

After calculating the difference in natural atomic charges (NAC, the nuclear charge minus the natural population sum of the natural atomic orbitals) observing the atoms X_2 and O_1 in the configuration of C_{2v} Δ [NAC (X_2) - NAC (O_1)], we found that this difference increases from compounds **1** to **4**. This trend can justify the hardness variation reduction ($\Delta\eta$) from compounds **1** to **4**. Also, the parameter Δ [NAC (X_2) - NAC (O_1)] can be considered as another criterion for estimating the PJT distortion in compounds **1** to **4**.

Table 6 LC-Wpbe /TZP-calculated stabilization energies (E_2 , in kcal mol⁻¹) associated with electron delocalizations, natural bond orders (NBO), natural atomic charges (NAC) and dipole moments (μ , in Debye) for the bent (C_{2v}) geometries of compounds 1-4

Geometry	1		2		3		4	
	C_{2v}	$D_{\infty h}$	C_{2v}	$D_{\infty h}$	C_{2v}	$D_{\infty h}$	C_{2v}	$D_{\infty h}$
	E_2							
LP ₂ O ₁ →σ* _{X2-03}	22.85	15.04	36.28	15.92	32.10	13.29	22.77	10.98
LP ₃ O ₁ →π* _{X2-03}	352.19	301.07	134.23	120.31	151.08	133.52	108.67	96.61
π _{O1-X2} →p ₍₀₃₎	14.39	11.70	-	-	0.00	-	0.00	-
σ _{O1-X2} →π* _{X2-03}	-	5.37	1.31	61.88	1.88	59.33	1.50	41.66
NBO								
σ _{O1-X2} (total)	1.3957		1.5000		1.5000		1.5000	
σ _{O1-X2} (ionic)	0.3148		0.6706		0.6753		0.7308	
σ _{O1-03} (covalent)	0.2086		0.0000		0.0000		0.0000	
NAC								
O ₁	-0.17008		-0.79888		-0.86557		-0.95164	
X ₂	0.34017		1.59775		1.73113		1.90328	
NAC(X ₂)-NAC(O ₁)	0.51025		2.39663		2.5967		2.85492	
μ	0.6706	0.0000	1.7517	0.0000	2.8723	0.0000	4.1416	0.0000
	(0.58±0.05) ^a		(1.634) ^{b,c}		(2.62±0.05) ^d		-0.95164	
	(0.5324±0.0024) ^e							

**FIGURE 3** The natural resonance theory (NRT) module provides an analysis of the molecular electron density (correlated or uncorrelated) in terms of resonance structures and weight. One of the possible reasons for justifying the absence of O₃ in the other molecules processes includes the presence of an additional resonance form (Figure 3), which was not observed for other molecules.

Conclusion

The purpose of this study was to investigate the stability of the curved form (C_{2v}) of XO_2 molecules ($X = O, S, Se, Te$) with theory levels of (LC-wPBE / Def2-TZVPP, B3LYP / Def2-TZVPP) and indicated that in all the molecules studied, stability level increases with reduction in the symmetry level. The elevated stability is attributed to the PJTE. The vibronic coupling interaction between the ground (Σ_g), and the first excited states (Π_u) throughout

the PJTE problem ($PJT(\Sigma_g + \Pi_u) \times \Pi_u$) is because of the asymmetry and molecules bending phenomenon. An increase in the stability of curved configurations (C_{2v}) in comparison with the linear configurations ($D_{\infty h}$) is compatible with the minimum energy principles (MEP) and maximum hardness principles (MHP).

Acknowledgements

Authors acknowledge for helpful comments of the peer reviewers.

Orcid:

Reza Fazaeli: <https://orcid.org/0000-0001-6498-2048>

Ali Esmaeili: <https://orcid.org/0000-0002-5076-2535>

References

- [1] I.B. Bersuker, *The Jahn–Teller Effect*, Cambridge University Press, Cambridge, UK, **2006**.
- [2] K.J. Donald, W.H. Mulder, L.V. Szentpaly, *J. Chem. Phys.*, **2003**, *119*, 5423–5436.
- [3] L. Margules, E. Herbst, V. Ahrens, F. Lewen, G. Winnewisser, H.S.P. Muller, *J. Mol. Spectrosc.*, **2002**, *211*, 211–220.
- [4] V. Ossenkopf, H.S.P.M. Müller, D.C. Lis, P. Schilke, T. A. Bell, S. Bruderer, E. Bergin, C. Ceccarelli, C. Comito, J. Stutzki, A. Bacman, A. Baudry, A.O. Benz, M. Benedettini, O. Berne, G. Blake, A. Boogert, S. Bottinelli, F. Boulanger, S. Cabrit, P. Caselli, E. Caux, J. Cernicharo, C. Codella, A. Coutens, N. Crimier, N.R. Crockett, F. Daniel, K. Demyk, P. Dieleman, C. Dominik, M.L. Dubernet, M. Emprechtinger, P. Encrenaz, E. Falgarone, K. France, A. Fuente, M. Gerin, T.F. Giesen, A.M. di Giorgio, J.R. Goicoechea, P.F. Goldsmith, R.G. Gusten, A. Harris, F. Helmich, E. Herbst, P. Hily-Blant, K. Jacobs, T. Jacq, C. Joblin, D. Johnstone, C. Kahane, M. Kama, T. Klein, A. Klotz, C. Kramer, W. Langer, B. Lefloch, C. Leinz, A. Lorenzani, S. D. Lord, S. Maret, P.G. Martin, J. Martin-Pintado, C. McCoey, M. Melchior, G.J. Melnick, K.M. Menten, B. Mookerjea, P. Morris, J.A. Murphy, D.A. Neufeld, B. Nisini, S. Pacheco, L. Paganani, B. Parise, J.C. Pearson, M. Pérault, T.G. Phillips, R. Plume, S. Quin, R. Rizzo, M. Röellig, M. Salez, P. Saraceno, S. Schlemmer, R. Simon, K. Schuster, F.F.S. van der Tak, A.G.G.M. Tielens, D. Teyssier, N. Trappe, C. Vastel, S. Viti, V. Wakelam, A. Walters, S. Wang, N. Whyborn, M. van der Wiel, H.W. Yorke, S. Yu, J. Zmuidzinas, *Astron. Astrophys.*, **2010**, *518*, L111/111–L111/115.
- [5] D.E. Woon, E. Herbst, *Astrophys. J. Suppl. Ser.*, **2009**, *185*, 273–288.
- [6] W.C. Gardiner, *Gas-Phase Combustion Chemistry*, Second ed., Springer-Verlag, New York, **2000**.
- [7] D. Rehder, *Wiley-WCH, Weinheim*, **2010**.
- [8] I.B. Bersuker, *Chem. Rev.*, **2013**, *113*, 1351–1390.
- [9] I.B. Bersuker, *Phys. Rev. Lett.*, **2012**, *108*, 137202.
- [10] H. Köppl, D.R. Yarkoni, L. Barentzen, (Eds.), *The Jahn-Teller Effect: Fundamentals and Implications for Physics and Chemistry*, Springer-Verlag Berlin Heidelberg, **2009**.
- [11] H. Kayi, P. Garcia Fernandez, I.B. Bersuker, J.E. Boggs, *J. Phys. Chem. A.*, **2013**, *117*, 8671–8679.
- [12] H. Kayi, I.B. Bersuker, J.E. Boggs, *J. Mol. Struct.*, **2012**, *1023*, 108–114.
- [13] Y. Liu, I.B. Bersuker, W. Zou, J.E. Boggs, *J. Chem. Theory Comput.*, **2009**, *5*, 2679–2686.
- [14] W. Zou, M. Filatov, D. Cremer, *Int. J. Quant. Chem.*, **2012**, *112*, 3277–3288.
- [15] P. Garcia Fernandez, Y. Liu, I.B. Bersuker, J.E. Boggs, *Phys. Chem. Chem. Phys.*, **2011**, *13*, 3502–3513.
- [16] P.G. Fernandez, I.B. Bersuker, J.E. Boggs, *J. Phys. Chem. A.*, **2007**, *111*, 10409–10415.
- [17] Y. Liu, I.B. Bersuker, W. Zou, J.E. Boggs, *J. Chem. Phys.*, **2010**, *376*, 30–35.
- [18] Y. Liu, *J. Comput. Theory Chem.*, **2014**, *1044*, 94–100.
- [19] K. Hajhoseinzadeh, R. Ghiasi, A. Marjani, *Eurasian Chem. Commun.*, **2020**, *2*, 78–86.
- [20] E. Faramarzi, R. Ghiasi, M. Abdoli-Senejani, *Eurasian Chem. Commun.*, **2020**, *2*, 187–195.
- [21] M. Vafaei-Nezhad, R. Ghiasi, F. Shafiei, *Chem. Methodol.*, **2020**, *4*, 161–171.
- [22] S. Ghorbaninezhad, R. Ghiasi, *Chem. Methodol.*, **2020**, *4*, 80–91.
- [23] G.G. Shalmani, R. Ghiasi, A. Marjani, *Chem. Methodol.*, **2019**, *3*, 752–767.
- [24] R. Ghiasi, A.H. Hakimioun, *Iran. Chem. Commun.*, **2017**, *5*, 67–78.

- [25] R. Ghiasi, M. Monajjemi, E.E. Mokarram, P. Makkipour, *J. Structural Chemistry*, **2008**, *49*, 600-605.
- [26] R. Ghiasi, H. Pasdar, *Russ. J. Phys. Chem. A*, **2013**, *87*, 973-978.
- [27] R. Ghiasi, H. Pasdar, F. Irajizadeh, *J. the Chilean Chemical Society*, **2015**, *60*, 2740-2746.
- [28] R. Ghiasi, F. Zafarniya, S. Ketabi, *Russ. J. Inorg. Chem.*, **2017**, *62*, 1371-1378.
- [29] R. Ghiasi, A. Heidarbeigi, *Russ. J. Inorg. Chem.*, **2016**, *61*, 985-992.
- [30] M. Rezazadeh, R. Ghiasi, S. Jamehbozorgi, *J. Structural Chemistry*, **2018**, *59*, 245-251.
- [31] G. Mahmoudzadeh, R. Ghiasi, H. Pasdar, *J. Structural Chemistry*, **2019**, *60*, 736-745.
- [32] G. Mahmoudzadeh, R. Ghiasi, H. Pasdar, *Russ. J. Phys. Chem. A*, **2019**, *93*, 2244-2249.
- [33] N. Najjari Milani, R. Ghiasi, A. Forghaniha, *J. Sulfur Chemistry*, **2018**, *39*, 665-673.
- [34] M. Nilchi, R. Ghiasi, E. Mohammadi Nasab, *Mol. Phys.*, **2019**, *117*, 567-574.
- [35] M. Nilchi, R. Ghiasi, E.M. Nasab, *J. the Chilean Chemical Society*, **2019**, *64*, 4360-4364.
- [36] F. Weigend, R. Ahlrichs, *Phys. Chem. Chem. Phys.*, **2005**, *7*, 3297-3305.
- [37] A.D. Becke, *J. Chem. Phys.*, **1993**, *98*, 1372-1377.
- [38] M.J. Frisch, G.W. Trucks, H.B. Schlegel, G.E. Scuseria, M.A. Robb, J.R. Cheeseman, G. Scalman, V. Barone, B. Mennucci, G.A. Petersson, H. Nakatsuji, M. Caricato, X. Li, H.P. Hratchian, A.F. Izmaylov, J. Bloino, G. Zheng, J.L. Sonnenberg, M. Hada, M. Ehara, K. Toyota, R. Fukuda, J. Hasegawa, M. Ishida, T. Nakajima, Y. Honda, O. Kitao, H. Nakai, T. Vreven, J.A. Montgomery, Jr. Peralta, J.E. Ogliaro, F. Bearpark, M. Heyd, J.J. Brothers, E. Kudin, K.N. Staroverov, V.N. Kobayashi, R.J. Normand, K. Raghavachari, A. Rendell, J.C. Burant, S.S. Iyengar, J. Tomasi, M. Cossi, N. Rega, J.M. Millam, M. Klene, J.E. Knox, J.B. Cross, V. Bakken, C. Adamo, J. Jaramillo, R. Gomperts, R.E. Stratmann, O. Yazyev, A.J. Austin, R. Cammi, C. Pomelli, J.W. Ochterski, R.L. Martin, K. Morokuma, V.G. Zakrzewski, G.A. Voth, P. Salvador, J.J. Dannenberg, S. Dapprich, A.D. Daniels, O. Farkas, J.B. Foresman, J.V. Ortiz, J. Cioslowski, D.J. Fox, *Gaussian09*, Revision A.02; Gaussian, Inc.:Wallingford CT, **2009**.
- [39] O.A. Vydrov, G.E. Scuseria, *J. Chem. Phys.*, **2006**, *125*, 234109.
- [40] A.E. Reed, L.A. Curtiss, F. Weinhold, *Chem. Rev.*, **1998**, *88*, 899-926.
- [41] G. Kouchzadeh, D. NoriShargh, *phys. Chem. Chem. Phys.*, **2015**, *17*, 29251-29261.
- [42] M. Karni, Y. Apeloig, *J. Am. Chem. Soc.*, **1990**, *112*, 8589-8590.
- [43] K.C. Mondal, B. Dittrich, B. Maity, D. Koley, H.W. Roesky, *J. Am. Chem. Soc.*, **2014**, *136*, 9568-9571.
- [44] I.B. Bersuker, *Chem. Rev.*, **2001**, *101*, 1067-1114.
- [45] R.G. Parr, R.G. Pearson, *J. Am. Chem. Soc.*, **1983**, *105*, 7512-7516.
- [46] R.G. Pearson, *J. Chem. Educ.*, **1999**, *76*, 267-275.
- [47] M. Torrent Sucarrat, M. Duran, M. Sola, *J. Phys. Chem. A*, **2002**, *106*, 4632-4638.
- [48] J. Onoda, M. Ondacek, P. Jelinek, Y. Sugimoto, *Nat. Commun.*, **2017**, *8*, 15155(1)-15155(6).

How to cite this article: Ali Esmaeli, Reza Fazaeli*, Esmat Mohammadi Nasab. Quantum chemical study of the Jahn – Teller effect on the distortions of XO₂ (X = O, S, Se, Te) systems. *Eurasian Chemical Communications*, 2020, 2(7), 739-749.
Link:
http://www.echemcom.com/article_105457.html